A three-dimensional analysis of acoustic propagation in a penetrable wedge slice

Grant B. Deane
Marine Physical Laboratory, Scripps Institution of Oceanography, La Jolla, California 92093

Chris T. Tindle
Physics Department, University of Auckland, Auckland, New Zealand

(Received 10 December 1991; accepted for publication 18 May 1992)

A model for the three-dimensional acoustic field in a penetrable wedge with isovelocity sound-speed profiles and a harmonic, point source is developed using the method of source images. The model is used to compute the field in a plane normal to the wedge apex (a wedge "slice"). A new loss term due to three-dimensional effects is derived and investigated. The field in the sediment of a wedge slice is computed and the mode penetration angles are compared with those obtained by Jensen and Kuperman [J. Acoust. Soc. Am. **67**, 1564–1566 (1980)] using the narrow angle parabolic equation and Jensen (private communication) using a coupled mode calculation.

PACS numbers: 43.30.Cq, 43.30.Bp, 43.30.Dr

INTRODUCTION

As a propagation problem, the two-dimensional wedge with a penetrable bottom poses some interesting difficulties. The nonseparability of the wave equation in this geometry has resulted in a number of approximate numerical and analytical techniques being developed to compute the acoustic pressure field. For a recent collection of analytical and numerical models applied to the penetrable wedge, the reader is referred to "Solutions to range-dependent underwater acoustics benchmark problems."[1]

In what follows we will be concerned with the general formulation of a model for the acoustic field in a penetrable wedge by employing the concept of source images. An analysis of this sort leads naturally to the concept of beam-displaced rays, which have been discussed by Brekhovskikh and Lysanov[2] and developed extensively by Tindle and coworkers[3–5] for one- and two-dimensional shallow-water field calculations.

The first successful application of beam-displaced rays to the penetrable wedge was the work of Tindle and Deane,[4] who considered both down-slope and up-slope propagation. More recently Westwood,[6] and Plumpton and Tindle[5] have independently extended the idea of beam-displaced rays to complex rays. Westwood[7] subsequently applied this formulation to a two-dimensional analysis of up-slope propagation in the penetrable wedge.

The present work is a three-dimensional analysis of the penetrable wedge, based on concepts that ultimately lead to complex ray theory. Although the final form that we obtain for the acoustic field can be interpreted in terms of complex rays, we shall not do so. The ideas underlying complex rays have been discussed by earlier authors,[5,7] and we do not require them in our analysis.

The geometry of the problem, shown in Fig. 1, is as follows. We consider a point, harmonic source of angular frequency ω located in a wedge of fluid bounded above by a perfectly reflecting interface, and below by a second, different fluid. Both fluids are assumed to be homogeneous; the sound speed and density of the upper and lower fluids being c_1, ρ_1 and c_2, ρ_2, respectively. In what follows we shall make use of the parameters defined by $m \equiv \rho_2/\rho_1$ and $n \equiv c_1/c_2$. The geometry of the wedge is characterized by the wedge angle α_w between the surface and bottom interface.

I. THE METHOD OF SOURCE IMAGES

The method of source images is essentially nothing more than a statement of the principle of linear superposition. We simply assume that the total pressure field in the wedge can be expressed as a sum of contributions from acoustic energy that has left the source and undergone a specified number of interactions with the wedge boundaries. Each contribution can be identified with a source image, the position of which can be found by (possibly multiple) reflection of the source in the surface and bottom interfaces. A moments reflection will verify that the images lie on a circle centered on the wedge apex.

Figure 2 shows the source images and notation we have adopted for the wedge. The ordering we have chosen to identify a given source image is based on n_b, the number of reflections from the bottom interface. In general, for a given n_b there are four source images depending on n_s, the number of surface reflections and whether the first reflection occurred

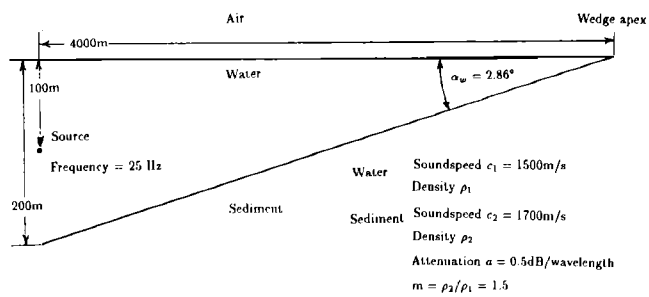

FIG. 1. Cross section of the geometry for the Acoustical Society of America benchmark wedge.

 0001-4966/92/091583-10$00.80 © 1992 Acoustical Society of America

wnloaded 01 Aug 2011 to 205.167.170.20. Redistribution subject to ASA license or copyright; see http://asadl.org/journals/doc/ASALIB-home/info/terms.

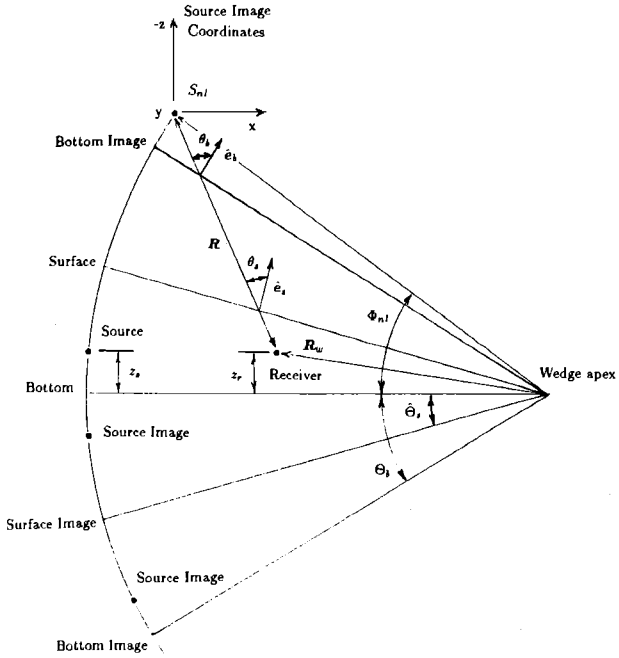

FIG. 2. The geometry of source images.

in the surface or bottom. Thus we require an additional parameter $l = -2, -1, 1, 2$, to identify an image uniquely. We have adopted the notation that $l < 0$ for images below the bottom and $l > 0$ for images above the bottom. We note that for $n_b = 0$ there are only two source "images"—an image from a single surface reflection and the source itself.

The angle of the source image corresponding to n_b bottom reflections and of type l is denoted by Φ_{nl} (see Fig. 2), and for the image itself we shall use the symbol S_{nl}. The interface image angles are denoted by Θ_b and $\hat{\Theta}_s$ for bottom and surface images respectively where $b = ..., -1,0,1, ...$ is the number of the bottom image and $s = ..., -1,0,1,...$ is the number of the surface image.

Let $p_{nl}(\mathbf{R}_w)$ be the (complex) acoustic field at the point $\mathbf{R}_w$ measured in wedge coordinates—see Fig. 2—due to the source S_{nl}. Then from the principle of linear superposition we express the total field at $\mathbf{R}_w$ as

$$P(\mathbf{R}_w) = \sum_{n_b=0}^{n_{\max}} \sum_{l} p_{nl}(\mathbf{R}) , \tag{1}$$

where $\mathbf{R}$ is the distance vector to $\mathbf{R}_w$ measured in source–image coordinates (x,y,z)—see below—and we are assuming that source images with $n_b > n_{\max}$ make a negligible contribution to the field. For realistic problems, attenuation due to multiple partial reflections with the bottom and geometric spreading of the wave field ensure that the sum in Eq. (1) converges.

There is an additional problem—apart from the matter of convergence—which needs to be considered when computing the field in a wedge with a source–image sum such as 1. Unless the wedge angle is an integer submultiple of π there exists some critical number of bottom reflections, n_{crit}, for which source images with $n_b > n_{\text{crit}}$ need to be treated as "imaginary" images.[8] Imaginary source images, first considered by Sommerfeld,[9] contribute to the diffracted component of the acoustic field. For the wedge regions and geometries we will be considering (away from the apex and small α_w) the diffracted component of the field is negligible and will not be considered.

To calculate each of the source–image contributions on the right-hand side of (1) we shall employ a generalization of the method Brekhovskikh and Lysanov[2] used to compute the field due to a single reflection of a harmonic spherical field from a two-fluid interface.

Let the source–image coordinates (x,y,z) be a Cartesian coordinate system centered on the source image of interest, with the x–y plane parallel to the bottom of the wedge, and the y axis parallel to the wedge apex. Then the spherical wave field due to the source image at the point $\mathbf{R} = x\hat{\mathbf{x}} + y\hat{\mathbf{y}} + z\hat{\mathbf{z}}$, where $\hat{\mathbf{x}}$, $\hat{\mathbf{y}}$, and $\hat{\mathbf{z}}$ are unit vectors parallel to the x, y, and z axis, respectively, is

$$p_{snl} = e^{ikR}/R , \tag{2}$$

where $k = \omega/c$ is the wave number, ω being the angular frequency of the source, c is the sound speed in the medium of propagation, and $R = \sqrt{x^2 + y^2 + z^2}$ is the distance from the point $\mathbf{R}$ to the source image. As we are dealing with planar boundaries, and know how to compute the interaction of plane waves with such boundaries, it is helpful to express p_{snl} as an integral of plane waves. The two-dimensional spatial Fourier transform of p_{snl} is $i/(2\pi k_z)$, so that

$$\frac{e^{ikR}}{R} = \frac{i}{2\pi} \int_{-\infty}^{\infty} \int_{-\infty}^{\infty} \frac{e^{i\mathbf{k}\cdot\mathbf{R}}}{k_z} dk_x\, dk_y , \tag{3}$$

where $\mathbf{k} = k_x\hat{\mathbf{x}} + k_y\hat{\mathbf{y}} + k_z\hat{\mathbf{z}}$ is the wave-number vector and $k_z = \sqrt{k^2 - k_x^2 - k_y^2}$. The kernel of this inverse Fourier transform consists of plane waves propagating in the direction of $\mathbf{k}$. As a given one of these plane waves propagates from the source image to the point $\mathbf{R}$, it undergoes n_b interactions with the bottom and n_s interactions with the surface. Each of these interactions is accounted for by multiplying the plane wave by the plane wave reflection coefficient for the interface (we are using the term "reflection" here loosely—for a plane wave that passes from the wedge interior into the sediment we would multiply by the transmission coefficient).

Let the reflection coefficients for the surface and bottom boundaries be denoted by $S(\theta_s)$ and $B(\theta_b)$, respectively, where

$$\theta_{s,b} = \cos^{-1}(\mathbf{k}\cdot\hat{\mathbf{e}}_{s,b}/k) \tag{4}$$

is the angle between the plane wave and a unit vector normal to the boundary; $\hat{\mathbf{e}}_s$ being normal to the surface and $\hat{\mathbf{e}}_b$ normal to the bottom. Given that the jth bottom image is at an angle Θ_b to the bottom, we can choose

$$\hat{\mathbf{e}}_b = -\sin\Theta_b\hat{\mathbf{x}} + \cos\Theta_b\hat{\mathbf{z}}. \tag{5}$$

It follows directly that

$$\cos\theta_b = (1/k)(-k_x \sin\Theta_b + k_z \cos\Theta_b) . \tag{6}$$

The corresponding expression for $\cos\theta_s$ is found by replacing Θ_b by Θ_s in Eq. (6) above.

Accounting for surface and bottom interactions, the field at the point $\mathbf{R}$ due to the source image S_{nl} is

wnloaded 01 Aug 2011 to 205.167.170.20. Redistribution subject to ASA license or copyright; see http://asadl.org/journals/doc/ASALIB-home/info/terms

$$p_{nl} = \frac{i}{2\pi} \int_{-\infty}^{\infty} \int_{-\infty}^{\infty} \prod_{s=1}^{n_s} S(\theta_s) \prod_{b=1}^{n_b} B(\theta_b) \frac{e^{i\mathbf{k}\cdot\mathbf{R}}}{k_z} dk_x\, dk_y \,. \tag{7}$$

Equation (7) for p_{nl}, when substituted into Eq. (1) for the total pressure field, represents a fully three-dimensional solution for the acoustic field in the water column and sediment of a penetrable wedge with isovelocity sound speed profiles.

While Eq. (7) may look simple enough, the double Fourier integral on the right-hand side is by no means trivial to evaluate. A similar integral appears when using the method of source images to find the acoustic field for the Pekeris model, where the boundaries are range independent. For this simpler geometry, it is possible to find a coordinate system (circular cylindrical coordinates) in which θ_s and θ_b depend on only one variable of integration, allowing one of the two integrals to be evaluated analytically. No such coordinate system exists for the penetrable wedge, and the angles $\theta_{s,b}$ will always be a function of both variables of integration. We can, however, make some analytical headway if we restrict consideration to propagation in a plane where $y = 0$. As we will show, even for this case there is a propagation loss due to three-dimensional effects.

II. PROPAGATION IN A WEDGE SLICE

We wish to investigate the solution for the acoustic field developed above for the case of up-slope propagation in a plane with unit normal parallel to the wedge apex, i.e., propagation directly up the wedge. As we shall show, if the receiver is restricted to such a plane that also contains the source, we can achieve a significant simplification in an asymptotic analysis of the field. We will refer to this special case as propagation in a wedge "slice."

Our ultimate aim here is to derive an asymptotic form for the double Fourier integral in (7) using the method of steepest descents. The first step in the analysis is to transform variables from Cartesian to circular cylindrical coordinates. Thus we set

$$\begin{aligned} k_z &= k\cos\theta, \quad z = R\cos\zeta, \\ k_x &= k\sin\theta\cos\phi, \quad x = R\sin\zeta\cos\xi, \\ k_y &= k\sin\theta\sin\phi, \quad y = R\sin\zeta\sin\xi. \end{aligned} \tag{8}$$

In the above transformations, ζ, ξ, and R are all fixed for a given source–receiver geometry. The variable ϕ measures the angle between the projection of $\mathbf{k}$ onto the x–y plane and the x axis, and θ corresponds to the angle between $\mathbf{k}$ and the z axis.

For the wedge slice, $y = 0$ and thus $\xi = 0$. The Jacobean for the transformation of $\mathbf{k}$ is $k^2 \sin\theta\cos\theta\, d\theta\, d\phi$, and with the appropriate change in limits, Eq. (7) can be rewritten as

$$p_{nl} = \frac{i}{2\pi} \int_0^{\pi/2 - i\infty} k\sin\theta\, d\theta \int_0^{2\pi} (-1)^{n_s} \times \prod_{b=1}^{n_b} B(\theta_b) e^{i\mathbf{k}\cdot\mathbf{R}}\, d\phi \,, \tag{9}$$

where

$$\mathbf{k}\cdot\mathbf{R} = \mathbf{k}\cdot\hat{\mathbf{z}}\hat{\mathbf{z}}\cdot\mathbf{R} + kR\sin\theta\sin\zeta\cos\phi \tag{10}$$

and, from (8) and (6) we have that

$$\cos\theta_b = \cos(\theta + \theta_b) + (1 - \cos\phi)\sin\theta\sin\Theta_b \,. \tag{11}$$

To obtain (9) we have made the assumption that the surface of the wedge is perfectly reflecting, and set $S(\theta_s) = -1$. We have left the $\hat{\mathbf{z}}$ component of the phase $\mathbf{k}\cdot\hat{\mathbf{z}}\hat{\mathbf{z}}\cdot\mathbf{R}$ in general form as this term depends on whether the receiver is in the water or the sediment, but is independent of ϕ. Continuity of the horizontal wave number $\mathbf{k}\cdot(\hat{\mathbf{x}} + \hat{\mathbf{y}})$ across the interface boundary ensures that the $\hat{\mathbf{x}}$ and $\hat{\mathbf{y}}$ phase terms are independent of the medium in which the receiver is placed.

From (11), it is clear that $\cos\theta_b$ depends on ϕ. It is this dependence between the angle of interaction with a bottom image and the azimuthal angle that complicates the three-dimensional analysis of the wedge. Were it not for this coupling, B would depend on θ alone and we could introduce a change of variables that would allow the integral over ϕ in Eq. (9) to be evaluated exactly analytically. As matters stand we must resort to a more approximate asymptotic evaluation.

In order to clarify the asymptotic analysis of Eq. (9), we will rewrite the integral over ϕ in the canonical form

$$p_{nl} = \frac{i}{2\pi} \int_0^{\pi/2 - i\infty} g(\theta) k\sin\theta\, d\theta \int_0^{2\pi} e^{i\Psi(\theta,\phi)}\, d\phi \,, \tag{12}$$

where

$$g(\theta) = (-1)^{n_s} e^{i\mathbf{k}\cdot\hat{\mathbf{z}}\hat{\mathbf{z}}\cdot\mathbf{R}} \,, \tag{13}$$

and

$$\Psi(\theta,\phi) = kR\sin\theta\sin\zeta\cos\phi - i\sum_{b=1}^{n_b} [\ln B(\theta_b)] \,. \tag{14}$$

We know from the method of steepest descents that the main contributions to the integral over ϕ in Eq. (12) occur at saddle points in the phase of the integrand in the (complex) ϕ plane. These points are solutions to

$$\frac{\partial\Psi(\theta,\phi)}{\partial\phi} = 0 \,. \tag{15}$$

Substituting Eq. (14) into Eq. (15) we obtain

$$-kR\sin\theta\sin\zeta\sin\phi - i\sum_{b=1}^{n_b} \left(\frac{1}{B(\theta_b)} \frac{dB(\theta_b)}{d\cos\theta_b} \frac{d\cos\theta_b}{d\phi} \right) = 0 \,, \tag{16}$$

where, from Eq. (4),

$$\frac{d\cos\theta_b}{d\phi} = \sin\Theta_b \sin\theta\sin\phi \,. \tag{17}$$

Clearly $\phi = 0, \pi, 2\pi$ are the three distinct solutions to Eq. (16) that lie in the range of integration of the integral over ϕ in (12), and are independent of θ. The saddle points at the two end points of integration will each contribute half of what either would add to the integral if it was in the interior of the range of integration.

For an isolated saddle point, the asymptotic form for the integral over ϕ obtained using the method of steepest descents is

$$I \simeq \sqrt{-2\pi/i\Psi_{\phi\phi}}\, e^{i\Psi_0} \,, \tag{18}$$

wnloaded 01 Aug 2011 to 205.167.170.20. Redistribution subject to ASA license or copyright; see http://asadl.org/journals/doc/ASALIB-home/info/terms.

where

$$\Psi_{\phi\phi} = \left.\frac{\partial^2 \Psi}{\partial \phi^2}\right|_{\phi = 0}, \tag{19}$$

and the subscript $_0$ denotes evaluation of the subscripted function at $\phi = 0$. Taking the second derivative of Ψ with respect to ϕ we obtain

$$\Psi_{\phi\phi} = -kR \sin\theta \sin\zeta \cos\phi - i \sum_{b=1}^{n_b} \left(\frac{1}{B(\theta_b)} \frac{dB(\theta_b)}{d\cos\theta_b} \frac{d^2 \cos\theta_b}{d\phi^2} \right), \tag{20}$$

where

$$\frac{d^2 \cos\theta_b}{d\phi^2} = \sin\Theta_b \sin\theta \cos\phi, \tag{21}$$

and we have set the terms involving $d\cos\theta_b/d\phi$ to zero. We can rewrite Eq. (20) as

$$\Psi_{\phi\phi} = -kR(1+\epsilon)\sin\theta \sin\zeta, \tag{22}$$

where

$$\epsilon = \frac{i}{kR \sin\zeta} \sum_{b=1}^{n_b} \left(\frac{1}{B(\theta_b)} \frac{dB(\theta_b)}{d\cos\theta_b} \sin\Theta_b \right). \tag{23}$$

Adding the contributions from the three saddle points, we obtain our final result

$$p_{nl} = i \int_0^{\pi/2 - i\infty} (-1)^{n_s} \left(\prod_{b=1}^{n_b} B(\theta_b) \right) \sqrt{\frac{1}{1+\epsilon}}\, e^{i\mathbf{k}\cdot\hat{\mathbf{z}}\hat{\mathbf{z}}\cdot\mathbf{R}} \times \sqrt{\frac{2}{\pi\varpi}} \cos\left(\varpi - \frac{\pi}{4}\right) k \sin\theta\, d\theta, \tag{24}$$

where

$$\varpi = kR \sin\theta \sin\zeta. \tag{25}$$

In order for the asymptotic analysis leading to Eq. (24) to be valid, we require the expansion parameter $kR \sin\zeta$ to be somewhat greater than unity. Thus we must satisfy the inequality

$$kR \sin\zeta \gg 1, \tag{26}$$

which amounts to requiring that the horizontal source–receiver separation be more than a few wavelengths.

The integral comprising our result differs in two respects from that obtained by Westwood[7] who considered propagation in a wedge slice, but assumed circular symmetry about the z axis. The first difference is the cosine function, which appears in Westwood's result as a Bessel function. This difference occurs as a result of our three-dimensional treatment of the problem. The additional complications arising from a three-dimensional treatment prevented us from evaluating the integral over ϕ in (12) exactly, and an asymptotic form involving the cosine function resulted. We note, however, that the asymptotic expansion for the Bessel function J_0 is

$$J_0 = \sqrt{\frac{2}{\pi\varpi}} \cos\left(\varpi - \frac{\pi}{4}\right), \tag{27}$$

and thus, apart from the factor involving ϵ, the two forms for the field are equivalent for sufficiently large values of ϖ.

The second difference is the term involving the factor ϵ that, again, arose from three-dimensional considerations. This factor is discussed below.

III. THE FACTOR ϵ

The parameter ϵ in Eq. (24) for p_{nl} arose from including the three-dimensional nature of the wedge propagation problem in our asymptotic analysis. The term arose as a contribution to $\Psi_{\phi\phi}$ from the reflection coefficient product. As can be seen from Eq. (18), such a contribution to the second derivative of the phase changes the amplitude of the asymptotic form for the integral. The ϕ dependence of $V(\theta_b)$ causes reflected plane waves to constructively interfere in a manner that is different from the case when $V(\theta_b)$ is independent of ϕ. Thus the reduction in amplitude due to ϵ is a reflection effect, but does not arise from horizontal refraction or beam displacement.

There is no term analogous to ϵ in the (two-dimensional) Pekeris model, and so we might expect that for small wedge angles, or large source–receiver separations that ϵ will make a vanishing contribution to the field. We can make an estimate of ϵ as follows.

Unless we include attenuation in the sediment, ϵ has singularities at $\sin\theta_b = n$. We can allow for attenuation in the bottom by supposing n to be complex, so that

$$n = n_0(1 + i\beta), \tag{28}$$

where β is a real, positive constant. Measurements of the acoustic attenuation in various sediments made by Hamilton[10] show that β is approximately independent of frequency and takes on values in the range 3×10^{-3} to 6×10^{-2}. Suppose that a represents the loss (in dB) incurred by propagating through one wavelength of sediment. Then a is a dimensionless constant, related to β by

$$\beta = \frac{a}{2\pi} \frac{\ln(10)}{20}. \tag{29}$$

With attenuation introduced in this way, we can estimate the magnitude of ϵ as follows. In order to simplify the algebra, we will estimate ϵ for a receiver in the water. Thus we can set $B(\theta_b) = V(\theta_b)$ in Eq. (23), where

$$V(\theta) = \frac{m\gamma_1 - \gamma_2}{m\gamma_1 + \gamma_2}, \tag{30}$$

and

$$\gamma_1 = \cos\theta, \quad \gamma_2 = (n^2 - 1 + \cos^2\theta)^{1/2}. \tag{31}$$

Taking the derivative of $\ln V(\theta)$ with respect to $\cos\theta$, we obtain

$$\frac{V'}{V} = \frac{m\gamma_1' - \gamma_2'}{m\gamma_1 - \gamma_2} - \frac{m\gamma_1' + \gamma_2'}{m\gamma_1 + \gamma_2}, \tag{32}$$

where the prime denotes differentiation with respect to $\cos\theta$.

For small β, $|\gamma_2|$ has a minimum, $|\gamma_2|_{\min}$, near $\theta = \sin^{-1} n_0$, and it follows from Eq. (32) that $|V'/V|$ has a maximum value

$$\left|\frac{V'}{V}\right|_{\max} \simeq \frac{2}{m|\gamma_2|_{\min}}. \tag{33}$$

It is not difficult to show that

wnloaded 01 Aug 2011 to 205.167.170.20. Redistribution subject to ASA license or copyright; see http://asadl.org/journals/doc/ASALIB-home/info/terms

$$|\gamma_2|_{\min} = 2^{1/2}\beta\left(\frac{n_0^2(1-\beta^2)}{\beta^2} - 1\right)^{1/4}, \tag{34}$$

at

$$\theta = \sin^{-1}[n_0^2(1-\beta^2) - 2\beta^2]^{1/2}. \tag{35}$$

From Eq. (34), $|\gamma_2|_{\min} \simeq (2\beta n_0)^{1/2}$ from which it immediately follows that

$$\left|\frac{V'}{V}\right|_{\max} \simeq \frac{1}{m}\sqrt{\frac{2}{\beta n_0}}. \tag{36}$$

Substituting (36) into Eq. (23) for ϵ, we find that to satisfy $|\epsilon| \ll 1$, we require that

$$\frac{1}{kR\sin\zeta}\frac{2\theta_w}{\pi} n_b(n_b - 1) \ll \sqrt{\beta}. \tag{37}$$

To obtain (37) we have used the approximations

$$\sum_{b=1}^{n_b} \sin\Theta_b \simeq \frac{2\theta_w}{\pi} n_b(n_b - 1), \tag{38}$$

and $[2/(n_0 m)]^{1/2} \simeq 1$.

Note that Eq. (37) will be satisfied for vanishing attenuation for small wedge angles and large horizontal separation (in terms of wavelengths) between the source image and receiver. It is also apparent that the term becomes more important for increasing n_b. Substituting the parameters for the ASA benchmark wedge (see Fig. 1) into Eq. (37), we find that the source–image to receiver horizontal separation, $r_{sr} \gg 70$ m for $n_b \leqslant 5$. This condition is satisfied throughout the greater part of the benchmark wedge.

The effect of ϵ on the field calculations for the benchmark wedge has been investigated by including it in an analysis similar to that shown below. We found the additional loss due to ϵ to be negligible for the wedge parameters corresponding to the ASA benchmark. Consequently, we will neglect the effect of ϵ in what follows.

IV. ASYMPTOTIC ANALYSIS FOR THE FIELD IN THE WATER

We wish to take the analytical analysis of Eq. (24) for p_{nl} further, and derive a wholly analytical asymptotic expansion for the pressure field in the water. We can do this by another application of the method of steepest descents. Using the relation

$$\cos(\varpi) = \tfrac{1}{2}(e^{i\varpi} + e^{-i\varpi}) \tag{39}$$

we can change the contour of integration in Eq. (24) to obtain

$$p_{nl} = \frac{1}{2}\int_{-\pi/2+i\infty}^{\pi/2-i\infty} (-1)^{n_s}\left(\prod_{b=1}^{n_b} V(\theta_b)\right) e^{i\mathbf{k}\cdot\hat{\mathbf{z}}\hat{\mathbf{z}}\cdot\mathbf{R}} \times\sqrt{2/\pi\varpi}\, e^{i\varpi} k\sin\theta\, d\theta, \tag{40}$$

where ϖ is given by Eq. (25),

$$\mathbf{k}\cdot\hat{\mathbf{z}}\hat{\mathbf{z}}\cdot\mathbf{R} = kR\cos\theta\cos\zeta, \tag{41}$$

and $B(\theta_b) = V(\theta_b)$, the two-fluid plane wave reflection coefficient.

We can express Eq. (40) in the canonical form

$$p_{nl} = \int_{-\pi/2+i\infty}^{\pi/2-i\infty} f(\theta) e^{i\varphi(\theta)}\, d\theta, \tag{42}$$

where

$$f(\theta) = (-1)^{n_s}\sqrt{\frac{ik\sin\theta}{2\pi R\sin\zeta}}, \tag{43}$$

and

$$\varphi(\theta) = kR(\cos\theta\cos\zeta + \sin\theta\sin\zeta) - i\sum_{b=1}^{n_b} \ln V(\theta_b). \tag{44}$$

The main contributions to p_{nl} occur around those values of θ that satisfy

$$\frac{d\varphi(\theta)}{d\theta} = 0. \tag{45}$$

An investigation of Eq. (45) shows that for n_b bottom interactions, there are in general $n_b + 1$ saddle points. However, only two of these points make a significant contribution to the integral. This is because $n_b - 1$ of the saddle points result in more than one value of θ_b less than the critical angle of $V(\theta_b)$, resulting in multiple partial reflection and subsequent attenuation of the incident plane wave field. Whether the contribution of such points to the integral can be neglected or not depends on what is considered a "significant" contribution. Our results for the ASA benchmark wedge are generally within a dB of results obtained by Westwood.[7] The observed differences between the two calculations could be due to either the neglect of energy from multiple partial reflections or the necessarily approximate nature of our asymptotic analysis. Whatever the case, we suggest that the agreement is sufficiently good to justify the neglect of multiple partial reflections.

We proceed, then, by assuming that Eq. (45) has two solutions that can merge in the complex θ plane. An asymptotic analysis using the method of steepest descents of such an integral has been considered by Chester *et al.*[11] to obtain the first term for a uniformly valid asymptotic expansion. Plumpton and Tindle[5] applied this analysis to a single reflection from a two-fluid planar interface and found agreement with numerical calculations to within 0.5 dB and 5.0° for a wide range of values of n and m.

Applying Plumpton and Tindle's analysis to Eq. (42), we obtain the asymptotic form

$$p_{nl} = 2\pi e^{i(\varphi_1+\varphi_2)}[P_0\,\mathrm{Ai}(-\sigma) + iQ_0\,\mathrm{Ai}'(-\sigma)], \tag{46}$$

where Ai and Ai′ are the Airy function and its derivative,

$$\sqrt{\sigma} = |\tfrac{3}{4}(\varphi_1 - \varphi_2)|^{\frac{2}{3}} e^{i[\arg(\varphi_1-\varphi_2)+2\pi]/3}, \tag{47}$$

and

$$P_0 = \tfrac{1}{2}(G_{\phi 1}G_{\theta 1} + G_{\phi 2}G_{\theta 2}),$$
$$Q_0 = (1/2\sqrt{\sigma})(G_{\phi 2}G_{\theta 2} - G_{\phi 1}G_{\theta 1}). \tag{48}$$

The factors G_ϕ and G_θ correspond physically to geometric spreading of the wave field in the ϕ and θ directions, respectively, and the subscripts $_{1,2}$ in Eqs. (46), (47), and (48) denote evaluation of the subscripted variable at each of the

wnloaded 01 Aug 2011 to 205.167.170.20. Redistribution subject to ASA license or copyright; see http://asadl.org/journals/doc/ASALIB-home/info/terms.

two points of stationary phase. The factors corresponding to geometric spreading are given by

$$G_\phi = f(\theta)\,,$$

$$G_\theta = \left(\frac{\pm 2\sqrt{\sigma}}{\varphi''}\right)^{1/2}, \quad -\frac{\pi}{2} < \arg(G_\theta) < \frac{\pi}{2}, \tag{49}$$

where $''$ denotes the second derivative with respect to θ.

Equation (46) for p_{nl} is a completely analytical solution for the contribution of each image source to propagation in the wedge slice, and will give an accurate value for the acoustic field provided the wedge parameters satisfy inequalities (26) and (37). This result is different from the analytical result previously developed by Tindle and Deane[4] in that the asymptotic form used is uniformly valid for small and large source–image to receiver horizontal separation and accounts for three-dimensional effects. We note that no special arguments have had to be employed to find the geometrical spreading of the wave fronts in the θ and ϕ directions. These have arisen as a natural consequence of our asymptotic analysis. We also note that although our result is analytical, it is still necessary to find the saddle points of Eq. (44) numerically. This is analogous to the sum of normal modes obtained for a Pekeris channel, which constitutes an analytical result although mode eigenvalues have to be obtained numerically.

V. THE FIELD IN THE SEDIMENT

We have investigated an asymptotic form for the pressure field in sediment similar to that derived for the water. We will not use the results of the analysis, but employ a more accurate numerical evaluation. The rationale for this is twofold. First, the partially reflected wave field that we neglected in the water makes a significant contribution to the field in the bottom and must be included in the calculations. This makes the asymptotic form more difficult to deal with and less practical to use. Second, and more importantly, we wish to compare our calculations with those of Jensen and Kuperman[12] made using the narrow angle parabolic equation, and Jensen[13] made using a coupled mode algorithm. Consequently, we wish to attain the greatest accuracy possible.

Neglecting the factor ϵ in Eq. (24), for the field in the sediment we have

$$p_{nl} = i\int_0^{\pi/2 - i\infty} (-1)^{n_s}\left(\prod_{b=1}^{n_b} B(\theta_b)\right) \times \sqrt{\frac{2}{\pi\varpi}}\cos\left(\varpi - \frac{\pi}{4}\right) k \sin\theta\, d\theta\,, \tag{50}$$

where ϖ is given by Eq. (25). In Eq. (50) the interaction coefficient B depends on b, the number of the bottom interaction. For $b > 1$, B is the plane wave reflection coefficient V, but for $b = 1$, B is the transmission coefficient defined by

$$W = 2m\gamma_1/(m\gamma_1 + \gamma_2)\,, \tag{51}$$

where γ_1 and γ_2 are defined in Eq. (31).

For the receiver in the sediment, we have that

$$\mathbf{k}\cdot\hat{\mathbf{z}}\hat{\mathbf{z}}\cdot\mathbf{R} = kz_s\cos\theta + kz_r\sqrt{n^2 - 1 + \cos^2\theta}\,, \tag{52}$$

where z_s is the height of the source image above the bottom and z_r is the depth of the receiver below the bottom. It is necessary to separate the phase into components above and below the bottom as the vertical wave number $\mathbf{k}\cdot\hat{\mathbf{z}}$ changes in passing from the water into the sediment on the final bottom interaction.

Equation (50), when substituted into Eq. (1) for the total pressure field, is a solution for the field in the sediment. In the sediment, energy arrives only from source images that lie above the bottom, and so the inner sum in (1) is restricted to values of $l > 0$.

VI. RESULTS

In order to satisfy inequality (26) for the wedge parameters we are concerned with, we require $\sim$200-m separation between the source and the receiver. Thus the approximations leading to Eq. (24) for the field in the water and sediment are not satisfied at very short ranges (< 200 m).

A. The field in the water

We have selected the ASA benchmark wedge as a test case for computing the field in the water column because it has already been studied with a number of analytical and numerical techniques. By obtaining agreement with this earlier work, we can demonstrate that the asymptotic form for the field in the water is accurate.

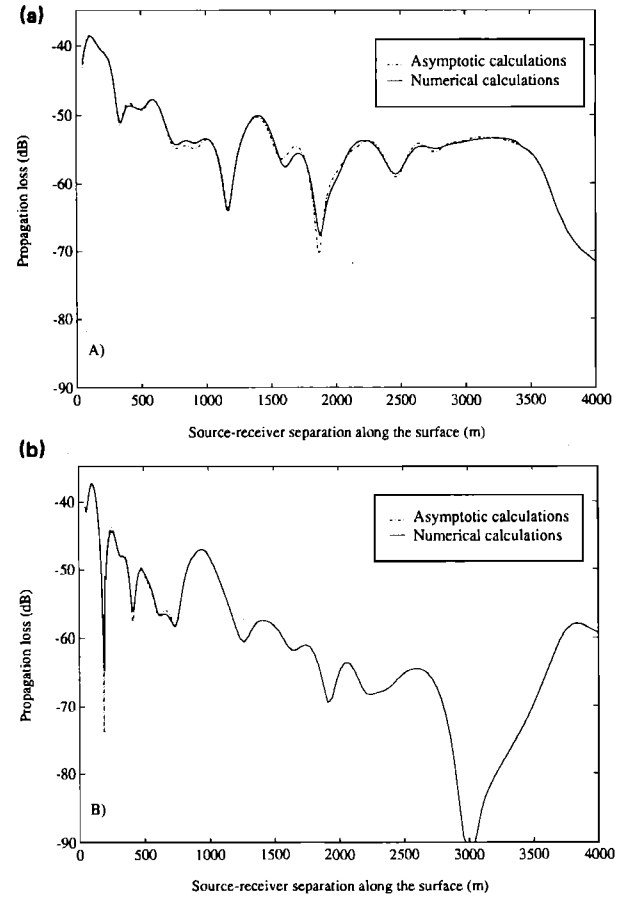

FIG. 3. Acoustic field amplitude in the Acoustical Society of America benchmark wedge for a constant receiver depth below the surface and no attenuation. The asymptotic calculations are compared with a numerical evaluation of the acoustic field. (a) Receiver 30 m below the surface. (b) Receiver 150 m below the surface.

wnloaded 01 Aug 2011 to 205.167.170.20. Redistribution subject to ASA license or copyright; see http://asadl.org/journals/doc/ASALIB-home/info/terms

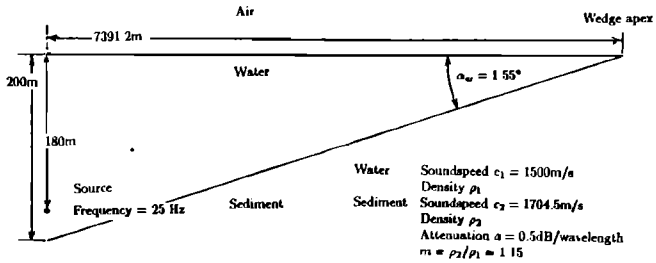

FIG. 4. Cross section of the geometry used to calculate the field in the Jensen and Kuperman wedge.

The results obtained using the asymptotic form and a numerical evaluation of the integral in Eq. (40) for the acoustic field in the ASA benchmark wedge geometry are shown in Fig. 3. We have also included a calculation of the field in the sediment, which was obtained by a numerical evaluation of Eq. (50). The parameters used for the calculations are shown in Fig. 1, with the attenuation factor $a = 0$.

The agreement between the new analytical form and the numerical evaluation is good, with the asymptotic calculations differing by a dB or so at some ranges.

B. The field in the sediment

The geometry used to calculate the field in the sediment of the Jensen and Kuperman wedge is shown in Fig. 4. The geometry differs from that used by Jensen and Kuperman in that we do not have a duct before the wedge. Even though the geometry is different the relative amplitudes of the three discrete modes are the same in both cases because the source is at the same position in the same depth of water.

Our results for the field are shown in Fig. 5. There is a continuum component that appears at short ranges in our results but has been eliminated by the duct in the Jensen and Kuperman case. Our field is similar to that of the Jensen and Kuperman case in that we also observe three lobes of energy in the sediment, each lobe corresponding to an intrinsic mode in the water column passing through its cutoff depth and penetrating the bottom. It is apparent from the results shown in Fig. 5 that both the lobe angles and positions are essentially the same as those obtained from the narrow angle parabolic equation model.

The agreement between the two sets of calculations demonstrates that the presence of the duct in the Jensen and Kuperman geometry has had no significant effect on the range at which modes penetrate the bottom, or their angle of penetration.

A more stringent test of the ray calculations is shown in Fig. 6. The reference calculations were kindly provided by Jensen,[13] who used a coupled mode calculation to obtain the field in the sediment for the geometry shown in Fig. 4. The agreement between the two contour plots is essentially exact with almost all of the features of the field reproduced down to the -90-dB level. The agreement between the two plots is encouraging as very different methods were used to arrive at the field.

While the contour line plots shown in Figs. 5 and 6 serve to show the gross features of the acoustic field in the sediment, they cannot reproduce the finer details that the field exhibits with any accuracy. To show these details we have

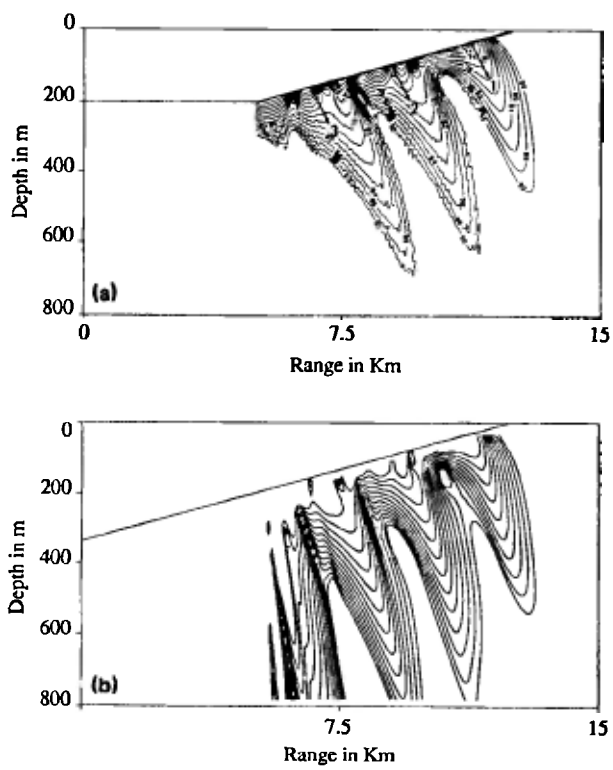

FIG. 5. Contour plot of the acoustic field amplitude in the Jensen and Kuperman wedge. (a) Jensen and Kuperman's results using the narrow angle parabolic equation. (b) Deane and Tindle's results.

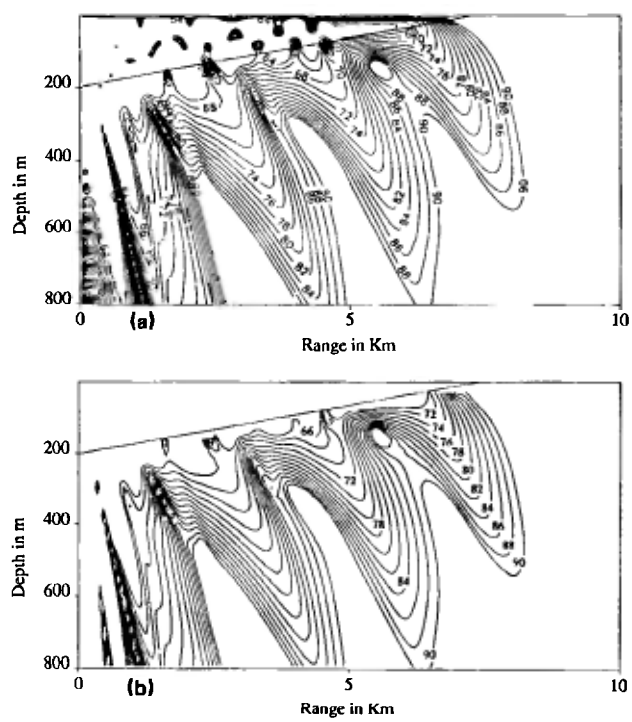

FIG. 6. Contour plot of the acoustic field amplitude in the Jensen and Kuperman wedge. (a) Jensen's reference calculations using a coupled mode model. (b) Deane and Tindle's results.

wnloaded 01 Aug 2011 to 205.167.170.20. Redistribution subject to ASA license or copyright; see http://asadl.org/journals/doc/ASALIB-home/info/terms.j

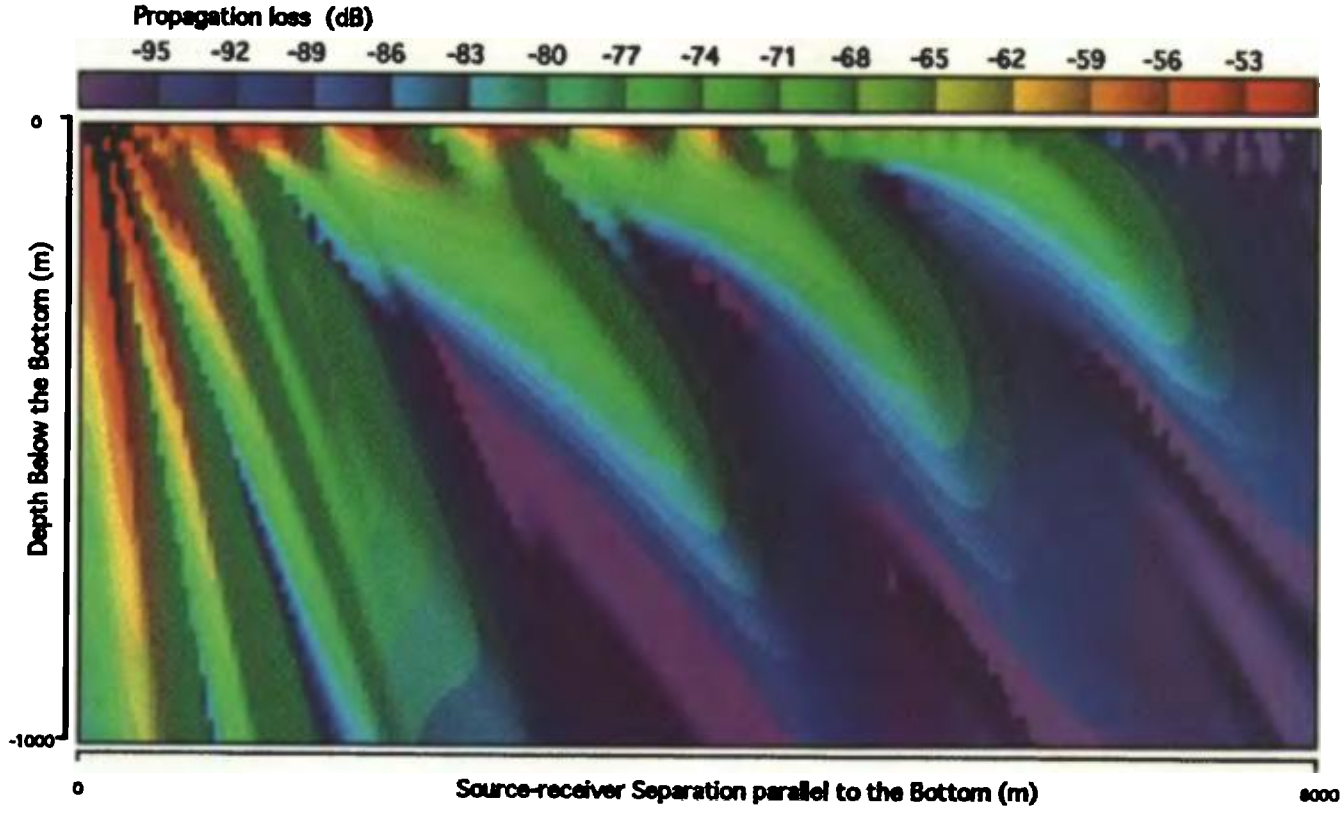

FIG. 7. Color contour plot of the propagation loss in the sediment of the Jensen and Kuperman wedge.

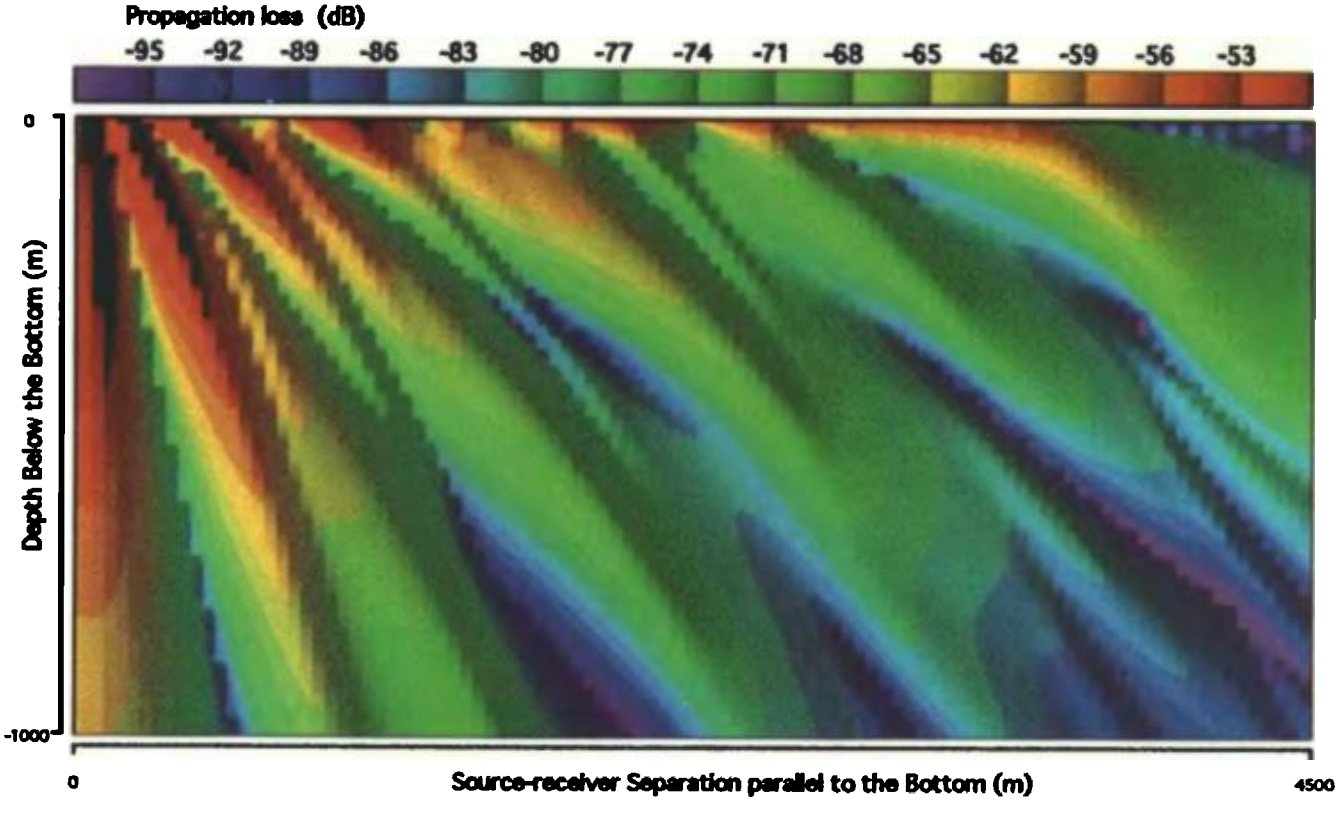

FIG. 8. Color contour plot of the propagation loss in the sediment of the Acoustical Society of America benchmark wedge.

nloaded 01 Aug 2011 to 205.167.170.20. Redistribution subject to ASA license or copyright; see http://asadl.org/journals/doc/ASALIB-home/info/term

included color contour plots; the field for the Jensen and Kuperman wedge is shown in Fig. 7. The absolute field levels are coded by color, and in addition the plot is shaded in the horizontal direction. The level of shading corresponds to the field gradient, and gives the plot a three-dimensional appearance. An examination of the plot shows that although there appears to be a well-defined angle associated with each lobe, in fact this angle is a function of depth below the wedge bottom. Furthermore, the second lobe from the right, corresponding to energy from mode two, shows evidence of bifurcating below 700 m.

To investigate the lobe structure and penetration angle as the wedge angle is increased we have plotted the field in the sediment of the ASA benchmark wedge. The parameters for the ASA benchmark wedge and the Jensen and Kuperman wedge are very similar, the main differences being the source position which is 100 m in the ASA wedge rather than 20 m, and the wedge angle which is 2.86° rather than 1.55°. The higher source position in the ASA benchmark wedge results in a weaker excitation of mode two. The results are shown in Fig. 8. The field pattern observed shows more structure than that seen in the narrower wedge. The lobes corresponding to modes three and two both loose their well-defined structure below about 500 m, and all the lobes have steeper angles of penetration (note that the horizontal scale for the plot is 4500 m whereas that for the narrower wedge is 8000 m). In addition to the changes in the lobes corresponding to the propagating intrinsic wedge modes, the energy corresponding to (evanescent) mode four is evident, as are fine-scale secondary interference maxima between lobes two and three, and lobes three and four (counting from right to left). These secondary maxima can also be seen in Fig. 7 although they are not as marked. Evidently, the field structure in the sediment is not as simple as Figs. 5 and 6 suggest, and becomes more complicated as the wedge angle is increased.

At least some of the structure exhibited by Figs. 7 and 8 can be explained in terms of source images. Each source image when viewed from the sediment has a "brightness" depending on the angle of the line that connects the viewing point to the source image. The source images that are brightest are those lying between the angles $\theta_c - 2\alpha_w$ and $\sim\theta_c + 10°$ (measured from the vertical). The energy from the source images at angles less than $\theta_c - 2\alpha_w$ undergoes multiple partial reflections before penetrating the bottom and is thus attenuated by bottom interactions. Energy from sources with angles greater than $\sim\theta_c + 10°$ has a long path in the bottom, and is attenuated by geometric spreading and absorption.

Consider a viewing point for a given depth moving from the source to the apex of the wedge. Near the source, the source images with small Φ_{nl}, corresponding to small n_b, are bright. As the viewing point is moved toward the apex these source images constructively and destructively interfere giving rise to the continuum. Further away from the source, there is an arc of adjacent sources that are bright and which interfere to give rise to the energy lobes corresponding to propagating intrinsic modes. The lobe corresponding to mode three in Fig. 8, for example, arises from the constructive interference of source images with $n_b = 2$, 3, and 4. The locus of the lobe maxima will be the path that corresponds to constructive interference for these sources, and a perspective for which they remain bright. The condition for the source images to remain bright suggests that the lobe angles will lie between $\theta_c - 2\alpha_w$ and $\sim\theta_c + 10°$, which is indeed the case.

As the viewing point is lowered, the interference pattern for a lobe becomes broader and eventually breaks apart into individual interference maxima arising from, in the case of lobe three for example, interference between source images with $n_b = 3{,}4$ and $n_b = 4{,}5$. As the wedge angle is increased, the source images are more widely spaced on the source–image circle and lobes separate into individual interference maxima at smaller depths.

VII. CONCLUSIONS

Our main result is the development of a *three-dimensional* model for the acoustic field in a wedge slice. Our analysis includes a new term due to three-dimensional effects. We have investigated the term, and found it to be unimportant for small wedge angles and in the far field.

We have demonstrated that it is possible to formulate an analytical ray model for the acoustic field in a wedge slice that yields the amplitude of the field to within a dB or so for the ASA benchmark geometry. As our model for the field in the water does not include energy from multiple partial reflections, our results show that these can be neglected unless accuracy to better than a dB is required. We also note that the geometrical factors associated with ray spreading, G_θ and G_ϕ, arose as a natural consequence of our analysis without the need to appeal to intuitive reasoning.

Our results for the lobe angles and positions in the sediment are the same as those obtained by Jensen and Kuperman,[12] and Jensen.[13] In the case of the coupled mode calculation the agreement of the field calculations is essentially exact.

ACKNOWLEDGMENTS

G. B. Deane is pleased to thank Professor Michael J. Buckingham for a number of helpful discussions, Professor L. C. Woods for his continuing support, and Jeff Sherman who wrote the color plotting software. We thank Finn Jensen for kindly providing the reference solution of Fig. 6. This work has been supported by the Mellon Foundation, Scripps Institution of Oceanography.

[1] "Solutions to range-dependent underwater acoustics benchmark problems," J. Acoust. Soc. Am. **87**, 1497–1545 (1990).
[2] L. Brekhovskikh and Yu. Lysanov, *Fundamentals of Ocean Acoustics*, Springer Series in Electrophysics (Springer-Verlag, New York, 1982).
[3] C. T. Tindle and G. E. J. Bold, "Improved ray calculations in shallow water," J. Acoust. Soc. Am. **70**, 813–819 (1981).
[4] C. T. Tindle and G. B. Deane, "Sound propagation over a sloping bottom using rays with beam displacement," J. Acoust. Soc. Am. **78**, 1366–1374 (1985).
[5] N. G. Plumpton, and C. T. Tindle, "Saddle point analysis of the reflected acoustic field," J. Acoust. Soc. Am. **85**, 1115–1123 (1989).
[6] E. K. Westwood, "Complex ray methods for acoustic interaction at a fluid-fluid interface," J. Acoust. Soc. Am. **85**, 1872–1884 (1989).
[7] E. K. Westwood, "Ray methods for flat and sloping shallow-water waveguides," J. Acoust. Soc. Am. **85**, 1885–1894 (1989).

ownloaded 01 Aug 2011 to 205.167.170.20. Redistribution subject to ASA license or copyright; see http://asadl.org/journals/doc/ASALIB-home/info/terms.js

[8] D. L. Bradley and A. A. Hudimac, "The propagation of sound in a wedge shaped shallow water duct," Naval Ordinance Laboratory Rep. No. NOLTR 70-235 (1970).
[9] A. Sommerfeld, "Mathematische Theorie der Diffraction," Math. Ann. **47**, 317–341 (1896).
[10] E. L. Hamilton, "Geoacoustic models of the sea floor," in *Physics of Sound in Marine Sediments*, edited by L. Hampton (Plenum, New York, 1974).
[11] C. Chester, B. Friedmann, and F. Ursell, "An extension of the method of steepest descents," Proc. Cambridge Philos. Soc. **53**, 599–611 (1957).
[12] F. B. Jensen and W. A. Kuperman, "Sound propagation in a wedge shaped ocean with a penetrable bottom," J. Acoust. Soc. Am. **67**, 1564–1566 (1980).
[13] F. B. Jensen (private communication).

wnloaded 01 Aug 2011 to 205.167.170.20. Redistribution subject to ASA license or copyright; see http://asadl.org/journals/doc/ASALIB-home/info/terms.